



Qia'erdunbasixi Fe–Cu Deposit in Sawur, Xinjiang: A Case Study of Skarn Deposit Hosted by Volcanic Rock

Shuang Yang¹, Qiu-Shi Zhou¹, Rui Wang^{1*} and Yongfeng Zhu^{2*}

¹State Key Laboratory of Geological Processes and Mineral Resources, and Institute of Earth Sciences, China University of Geosciences, Beijing, China, ²The Key Laboratory of Orogenic Belts and Crustal Evolution, Ministry of Education, School of Earth and Space Science, Peking University, Beijing, China

OPEN ACCESS

Edited by:

Hassan Mirnejad,
Miami University, United States

Reviewed by:

Xiao-Ping Xia,
Guangzhou Institute of Geochemistry
(CAS), China
Lejun Zhang,
University of Tasmania, Australia

*Correspondence:

Rui Wang
rw@cugb.edu.cn
Yongfeng Zhu
yfzhu@pku.edu.cn

Specialty section:

This article was submitted to
Economic Geology,
a section of the journal
Frontiers in Earth Science

Received: 11 January 2022

Accepted: 11 May 2022

Published: 24 June 2022

Citation:

Yang S, Zhou Q-S, Wang R and Zhu Y
(2022) Qia'erdunbasixi Fe–Cu Deposit
in Sawur, Xinjiang: A Case Study of
Skarn Deposit Hosted by
Volcanic Rock.
Front. Earth Sci. 10:852261.
doi: 10.3389/feart.2022.852261

The Sawur Cu–Au belt, northern Xinjiang, China, is the eastward extension of the Zarma–Sawur Cu–Au belt in Kazakhstan, where Late Paleozoic volcanic rocks and intrusions are highly developed. The Qia'erdunbasixi Fe–Cu deposit in Sawur is a recently discovered deposit and is still under exploration. The intrusive rocks are syenite and diorite, and the wall rocks consist of andesite and minor basalt, lamprophyre, and tuff. The U–Pb SHRIMP zircon age of the Qia'erdunbasixi syenite intruding into the volcanic rocks is 345 ± 2.2 Ma (MSWD = 1.3), presenting as the lower limit of skarn Fe mineralization. The intrusives belong to the calc–alkaline to high-K calc-alkaline series with large ion lithophile element (LILE) enrichment, high LREE/HREE fractionation, and high field strength element (HFSE) depletion. The initial $^{87}\text{Sr}/^{86}\text{Sr}$ ratios of the Qia'erdunbasixi syenite range from 0.70403 to 0.70420, and the $\epsilon_{\text{Nd}}(t)$ values are from +5.5 to +6.8, which are the typical characteristics of island arc igneous rocks. Diorites having similar REE features with syenite should share the same magma source. Magnetite and copper mineralization develop mostly along the contact zones of syenite and diorite, respectively. Fe mineralization develops along the contact zone of syenite, with typical skarn zonation. The metallogenesis event can be divided into the prograde skarn stage (diopside–augite–andradite–magnetite–calcite–quartz), retrograde skarn stage (epidote–chlorite–actinolite–K-feldspar–calcite–magnetite–quartz), and quartz–sulfide stage (quartz–magnetite–K-feldspar–calcite–sercite–chlorite–actinolite–prehnite–chalcopryite–pyrite). The early–mid-stage magnetite with certain amounts of Ti and V was crystallized from magma, while the late-stage magnetite has the typical characteristics of hydrothermal calcic skarn magnetite. The temperature of mineralization is between 350 and 450°C based on mineral assemblages and phase diagrams. Copper mineralization is concentrated along the outer contact zone of the diorite. Paragenesis sequences of the four stages of mineralization could be identified for copper mineralization: 1) albite–quartz; 2) chalcopryite–pyrite–gold–seriate–quartz; 3) chalcopryite–pyrite–epidotic–reunite; and 4) sphalerite–galena–quartz–calcite. Qia'erdunbasixi is a composite deposit with skarn-type Fe mineralization and mesothermal Cu mineralization and has a genetic relationship with magmatism in an island arc setting.

Keywords: skarn, magnetite, syenite, Sawur, island arc, Fe–Cu deposit

INTRODUCTION

Skarn deposits occur in both the contact zone with carbonate rocks and the contact zone with volcanic–sedimentary rocks, such as volcanic sedimentary tuff and andesite. Einaudi (1981) suggested that skarn deposits hosted in volcanic rocks should belong to the metasomatic skarn deposit. Zhao et al. (1990) classified this type into the skarn deposit related to volcanic gas and fluid. Such atypical skarn deposits mainly present as calcic iron skarn deposits, which are usually found in island arcs. The intrusive rocks are generally dioritic, sometimes also syenitic (Einaudi, 1981). British Columbia contains at least 147 recorded iron skarn deposits, wherein over 90% are hosted by Late Triassic limestone and volcanic rocks (Ray, 1995). Skarn minerals such as garnet and pyroxene hosted in volcanic rocks are different in their element compositions from those hosted in carbonate rocks (Meinert, 1984). Wall rock lithology plays an important role in the metallogenesis of skarn deposits. Carbonate rocks, such as limestone, dolomitic limestone, and dolomite are easily replaced because they are chemically active, brittle, easy to penetrate, and enriched in Ca. In contrast, volcanic rocks are less vulnerable to modification, but are richer in iron and mobile elements, such as K and Na. These atypical deposits hosted by volcanic rocks are petrologically and geochemically unique, and detailed studies are

needed to understand their genesis in comparison with typical skarn deposits.

The Sawur Cu–Au belt, an eastward extension of the Zarma–Sawur Au–Cu belt in Kazakhstan, is in the Sawur Mountains along the northwestern margin of the Junggar Basin, northern Xinjiang, China. A considerable quantity of gold and copper deposits is hosted in the volcanic rocks of the Sawur area (Yuan et al., 2015; Zhang, 2016; Xia et al., 2022). The Qia'erdunbasixi Fe–Cu deposit in Sawur is a newly discovered deposit (Wang and Zhu, 2007, 2010; Xia et al., 2022). The wall rocks mainly consist of andesite with minor basalt, lamprophyre, and tuff, intruded by syenite and diorite. Magnetite and chalcopyrite mineralization develops along the contact zone between intrusives (syenite and diorite) and andesite.

In this article, we report our studies of the Qia'erdunbasixi deposit with respect to deposit geology. We have conducted zircon U–Pb dating of syenite to better constrain the age of mineralization, and determine the whole major and trace elements, and radiogenic isotopes (Sr, Nd) of intrusions, and ore mineral geochemistry to constrain the origin of intrusions and the nature of the ore-forming fluid. This study reveals the genesis of the volcanic hosted Fe–Cu deposit and their controlling factors, and the proposed genetic model could be used to guide the exploration of potential Fe–Cu deposits in the Sawur area.

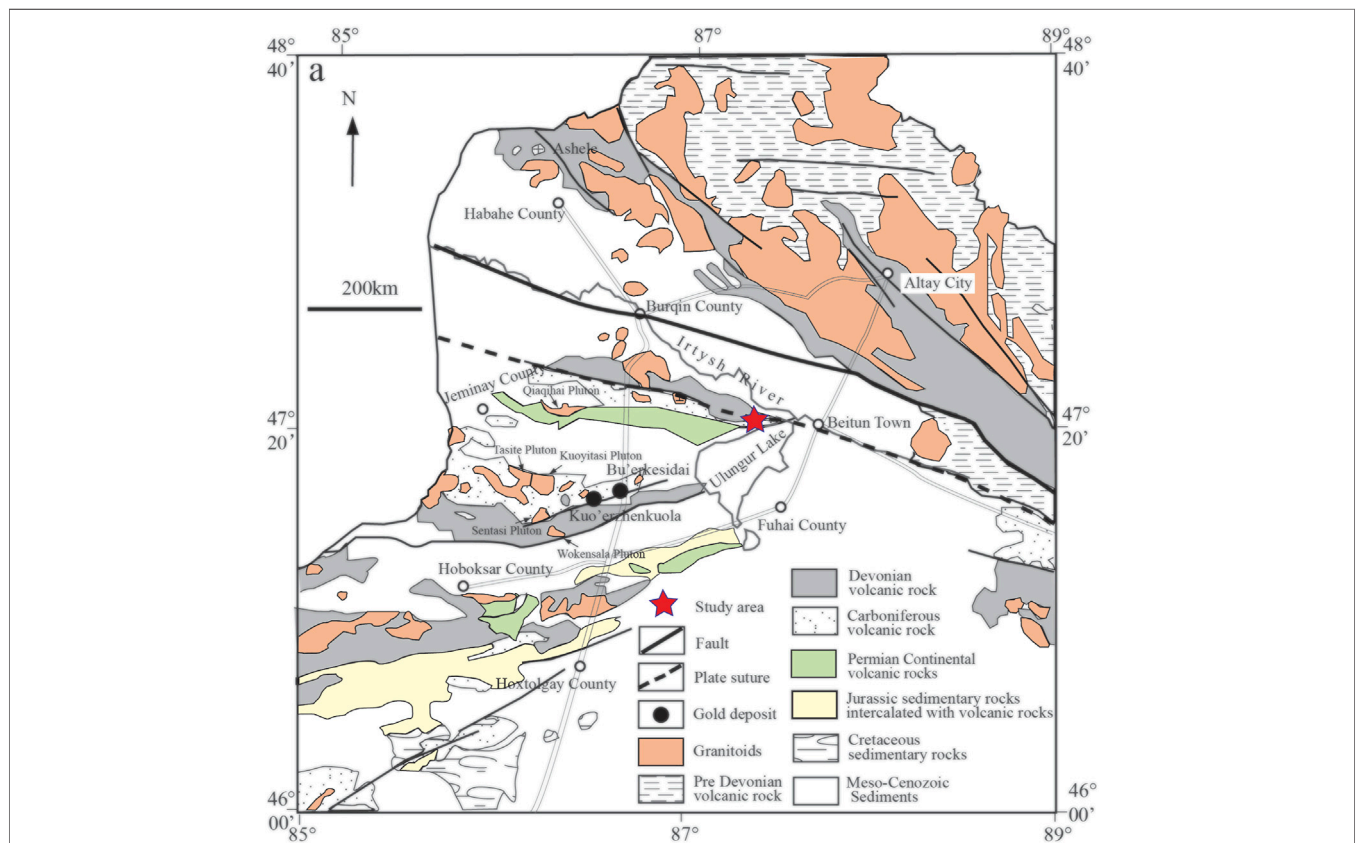
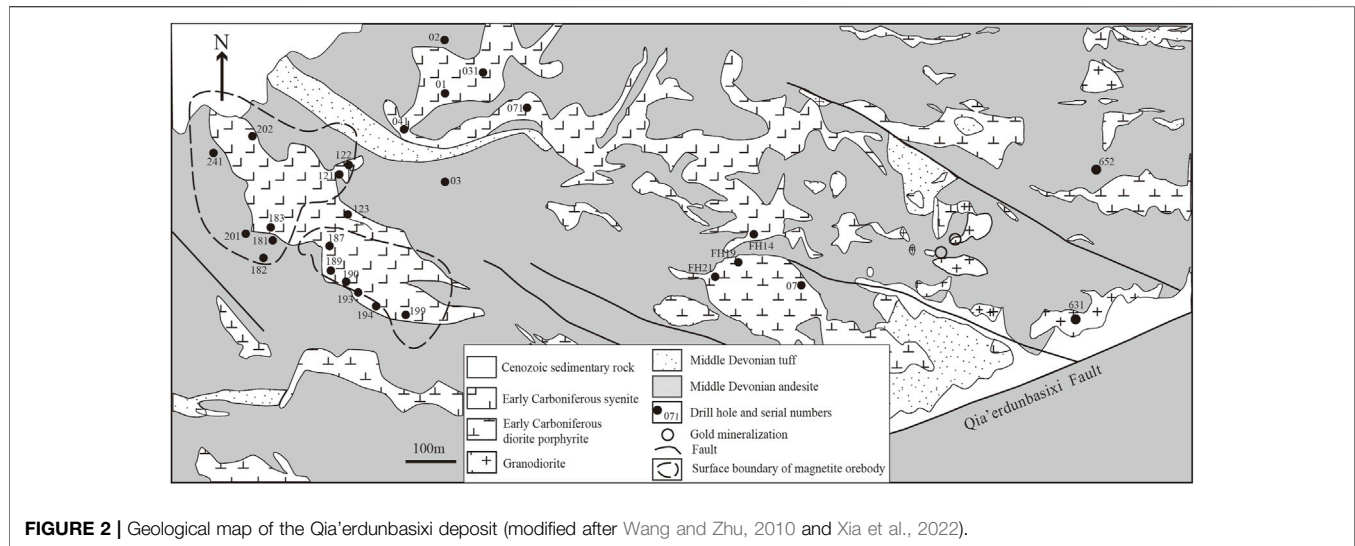


FIGURE 1 | Regional geological map of Sawur and adjacent regions (modified after He et al., 2005).



REGIONAL GEOLOGY

The Zharma–Sawur volcanic arc is separated by the Irtysh–Zaysan suture zone from the Altai orogen in the north (**Figure 1**). The NW–SE trending Irtysh–Zaysan suture zone is the product of a collision between the Altai and Kazakhstan blocks (e.g., Windley et al., 2007; Vladimirov et al., 2008; Chen et al., 2010; Zhu et al., 2016). In East Kazakhstan, abundant Late Devonian–Early Carboniferous conodonts and radiolarians were discovered in the silicic rocks of the Char ophiolite within the Irtysh–Zaysan suture zone (Iwata et al., 1994, 1997).

The Sawur region, an eastward extension of the Zarma–Sawur island arc belt in Kazakhstan, is located along the northwestern margin of the Junggar Basin (He et al., 1995; Windley et al., 2002; Zhu et al., 2013; 2015). The strata outcropping in the Sawur region consist of a Devonian–Carboniferous marine volcanic–sedimentary sequence, a Permian continental volcanic–sedimentary sequence, and Cenozoic sediments (Bureau of Geology and Mineral Resources of Xinjiang Uygur Autonomous Region, 1993). The Middle Devonian Sawur Formation, as the oldest in the Sawur district, mainly consists of volcanic rocks. The Burqin Formation in the later period of the Middle Devonian is a series of marine intermediate–basic volcanic clastic rocks and sedimentary clastic rocks. Upper Devonian Taerbahata is a set of volcanic flysch. The Lower Carboniferous Formations include the Heishantou, Halabayi, and Nalinkala Formations. The Heishantou Formation, hosting Buerkesidai and Kuozhenkuola gold deposits, consists of a succession of volcanic rocks and volcanic clastic rocks with an intercalation of limestone and siltstone, representing a typical island arc volcanic assemblage (Shen et al., 2007; Chen et al., 2017). The Rb–Sr isochron age of andesite in the Heishantou Formation is 342 Ma, and 325 Ma for sillite (He et al., 1994). The Upper Carboniferous sequences consist of the Sarbulake and Qiaqihai Formations. The Permian strata are made of volcanic–sedimentary rocks. The Harjiao Formation features continental volcanic rocks, and the

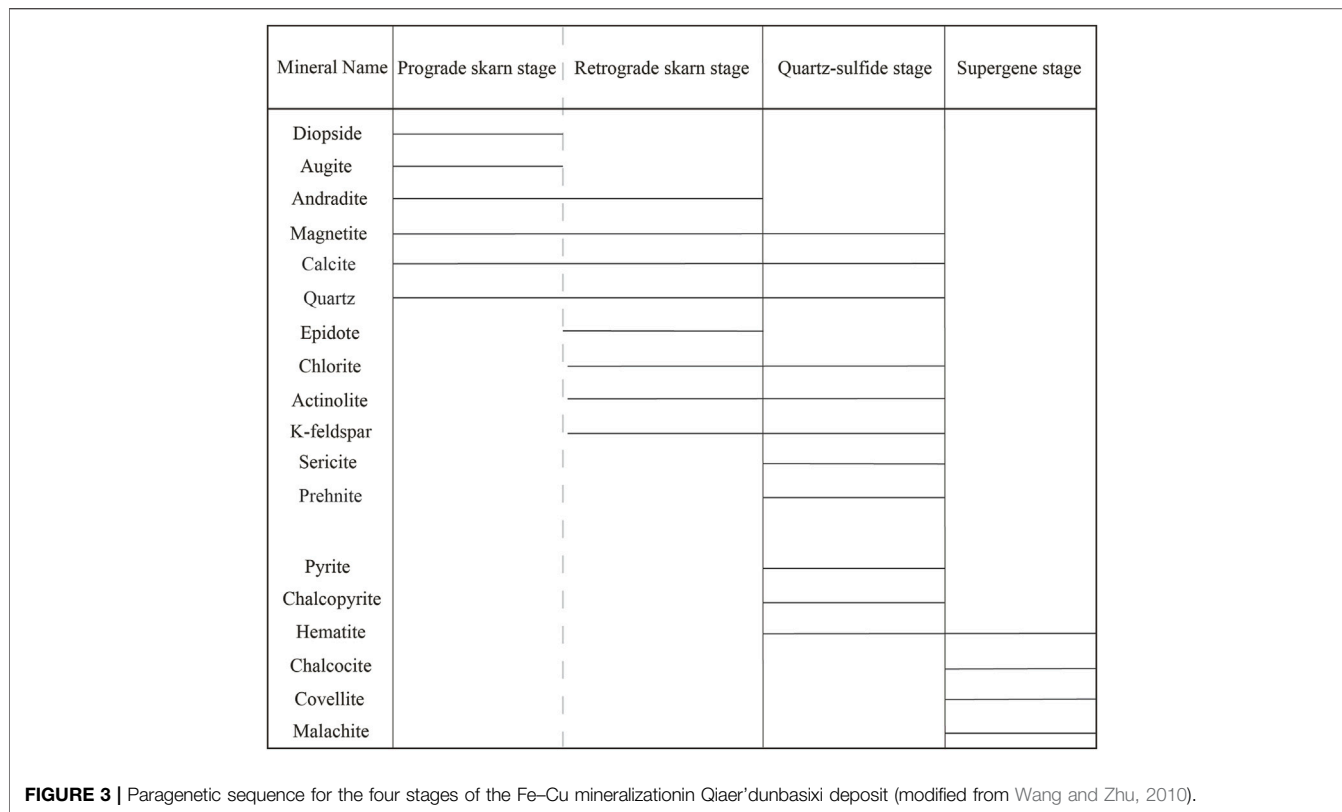
overlying Kalagan Formation, as volcanic rocks, has a typical bimodal characteristic (Zhou et al., 2006). The $^{40}\text{Ar}/^{39}\text{Ar}$ age of the volcanic rocks in the Kalagan Formation is between 283 and 280 Ma (Tan et al., 2007).

Granitic intrusions are widespread in the Sawur region. Based on previous work (Yuan et al., 2006; Zhou et al., 2006, 2008; Chen et al., 2010), these granitic intrusions can be subdivided into I-type granites (Tasite, Sentasi, Wokensala, and Kaerjia plutons) and A-type granites (Kuoyitasi and Qiaqihai plutons). The I-type granite consists of granite, granodiorite, and the A-type granite is mostly alkali granite. The SHRIMP U–Pb dating results indicate that the I-type granites were formed between 337 Ma and 302.6 Ma, and the A-type between 297.9 Ma and 290.7 Ma. From the oldest to the youngest granite, compositions vary from calc–alkaline to high-K calc–alkaline, to alkali series (Zhou et al., 2008).

Many gold deposits and other mineral occurrences are hosted in the volcanic rocks of the Sawur area, and together they define the EW-trending gold belt (Zhu et al., 2014; Xia et al., 2022). The Kuozhenkuola and Buerkesidai volcanogenic hydrothermal gold deposits are the two largest deposits in the belt (Shen et al., 2007), wherein gold mineralization is genetically associated with mantle-derived materials (Shen et al., 2008; Xia et al., 2022).

DEPOSIT GEOLOGY

The Qia'erdundasixi Fe skarn is located along the contact between syenite and Middle Devonian volcanic rocks, which are andesite interbedded with basalt, lamprophyre, and tuff as displayed in the Qia'erdundasixi deposit (**Figure 2**). In the mining area, the NE-trending Qia'erdundasixi fault and several NW-trending branch faults (**Figure 2**) are developed. The mineralization is featured by development in the contact zone between plutons and volcanic wall rocks. Magnetite mineralization is mainly developed in the internal and external contact zones of syenite; copper



mineralization is mainly developed in the external contact zone of diorite, and gold mineralization is closely related to granodiorite porphyry. In the Qia'erdundunbasixi area, the volcanic rock is in the second part of the Burqin Formation. This part comprises of dacite, rhyolite, tuffaceous breccia, and tuff, interbedding amygdaloid andesite, basalt, and minor lamprophyre. Andesite with minor basalt, tuff and rhyolite are the main wall rocks. Andesite develops a clear amygdaloidal structure and hyalopilitic texture, as well as minor pyrite–epidote veins. Amphiboles and minor plagioclases are the main phenocrysts in andesite, some amphiboles are replaced by epidotes and chlorites, as well as a minor development of quartz–calcite veins. The amygdule minerals include quartz, calcite, albite, epidote, and chlorite. Basalt, as a minor phase in the volcanic wall rocks, can be classified into two categories depending on their mineralogical features: 1) megacryst basalt is characterized by clinopyroxene megacrysts (5–10 mm) with a hyalopilitic texture, where albite microcrysts are also present. 2) Amphibole basalt is characterized by clinopyroxene and amphibole phenocrysts of 0.5–1.5 mm. The tuffs are highly brecciated andesite or diorite. There are quartz phenocrysts and minor fragments of plagioclase in rhyolite. Both tuff and rhyolite are highly developed with quartz and epidote veins.

The syenite consists of clinopyroxene, plagioclase, and minor apatite (~5 vol%), and magnetite (~5 vol%). Primary basic plagioclase is replaced initially by albite, calcite, and sericite, and then enclosed by K–feldspar. Some clinopyroxene rims are surrounded by large quantities of magnetite. There are two groups of magnetite, the former type is characterized by a larger

size (1 mm), abundant cracks, round shape, and cloudy face, indicating xenocrysts. The latter type is clean, euhedral, and small (<0.3 mm), and usually intergrown with chlorite and epidote.

Mineralization

Magnetite, copper, and gold mineralizations are well developed in the Qia'erdundunbasixi deposit. The late Paleozoic basalt, andesite, tuff, and volcanic breccia exposed in a large area in the Qia'erdundunbasixi mining area are intruded by diorite and syenite.

Copper mineralization is concentrated mainly in the outer contact zone of diorite, and most of the copper mineralization is filled in hydrothermal breccia, featuring a mesothermal hydrothermal vein copper deposit. Ore minerals mainly include pyrite, chalcopyrite, galena, and sphalerite, and Gangue minerals mainly include quartz, calcite, epidote, sericite, prehnite, chlorite, K-feldspar, albite, and pumpellyite. The ore structure is mainly disseminated veinlet and breccia structures. Diorite ore has a disseminated veinlet structure, while the andesite and tuff ores are mainly filled with chalcopyrite veinlets and pores. The main wall rock alteration types include sericite, epidote, K-feldspar, chlorite, quartz, and calcite alteration. Epidote and sericite alterations are closely related to chalcopyrite mineralization. Tuff and andesite are widely subjected to epidote and pyrite alteration, and the late quartz alteration is closely related to galena and sphalerite mineralization. Magnetite mineralization develops along the contact zone between syenite and volcanic rocks (dominated by andesite). There are two magnetite ore bodies shown in **Figure 2**. Ore types include massive and disseminated

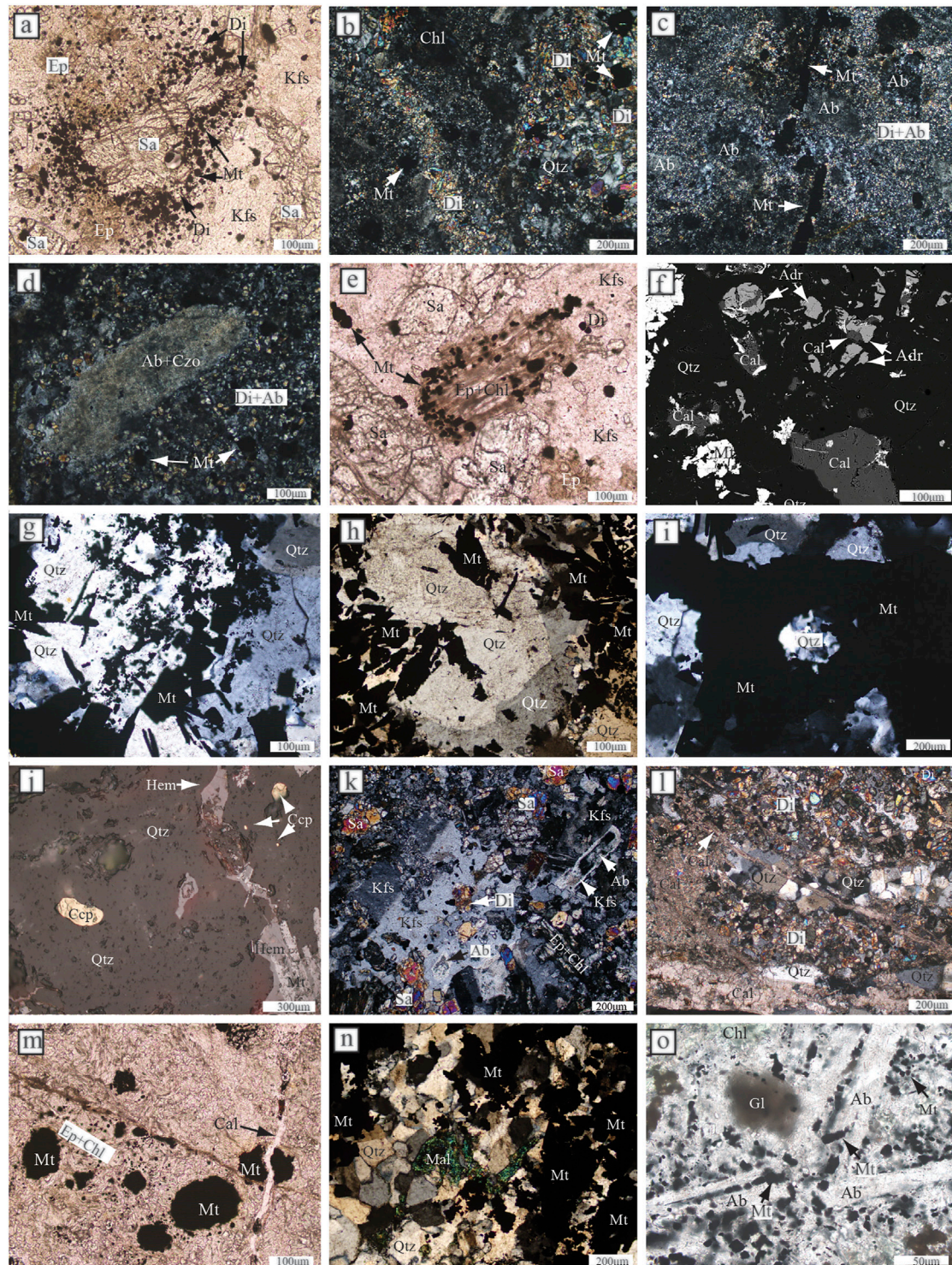
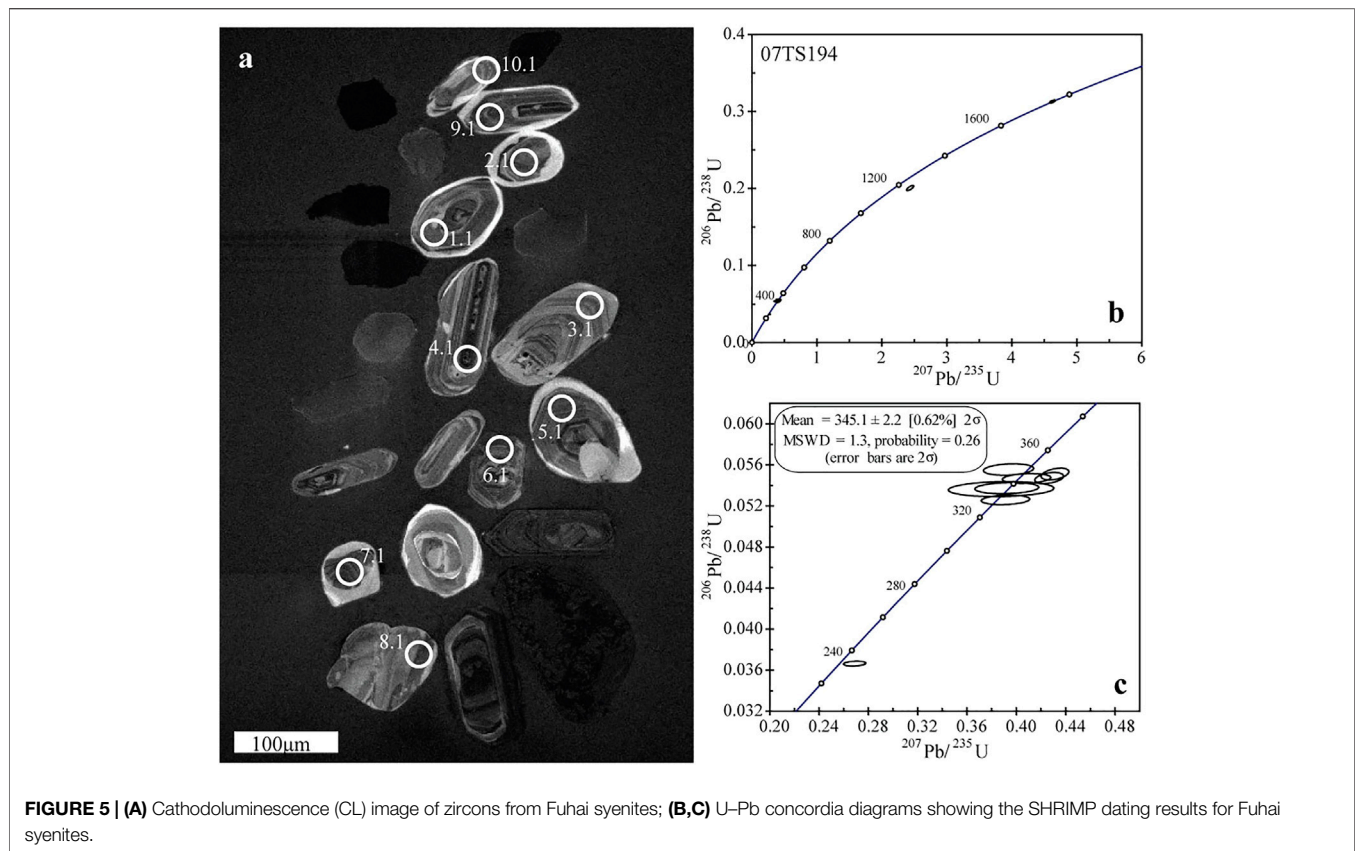


FIGURE 4 | (A) Clinopyroxene is densely disseminated or presents as veinlets near the contact zone; (B) Magnetite is sparsely disseminated; (C) Magnetite veinlets; (D) Clinopyroxene is metasomatized by epidote + chlorite + magnetite, and epidotization and chloritization in the outer contact zone are well developed; (E,I) Alterations of quartz + magnetite + K-feldspar + calcite + sericite + chlorite + prehnite + actinolite + chalcocyanite + pyrite are developed in the hydrothermal stage; (F,G) The quartz-magnetite vein with a width of about 2–10 cm, where magnetite accounts for as much as 40 vol% of the vein volume; (J) Chalcopyrite is disseminated and magnetite is metasomatized by hematite; (K,L) Coarse K-feldspar grain, with inclusions of diopside formed in the early stage; (M) The calcite vein formed in the latest stage cuts through the early-stage magnetite; (N) Malachite in the magnetite-quartz vein; (O) Wall rock of andesite is intensely mineralized with magnetite. Plane polarized light (A,E,M, and O), cross polarized light (B–D,G–I, K,L, and N), reflected light (J), and the BSE image (F). Ab—albite; Adr—andradite; Cal—calcite; Ccp—chalcopyrite; Chl—chlorite; Czo—clinzoisite; Di—diopside; Ep—epidote; Gl—glass; Hem—hematite; Mal—malachite; Mt—magnetite; Kfs—K-feldspar; Qtz—quartz; Sa—salite; Ser—sericite (modified after Wang and Zhu, 2010).



magnetite ore. The main ore minerals are magnetite and chalcopyrite, and the gangue minerals include pyrite, quartz, diopside, epidote, chlorite, actinolite, calcite, sericite, and andradite. The wall rock alteration is mainly skarn, quartz, chlorite, calcite, and sericite alterations.

Magnetite mineralization has distinctive zoning features. Through sampling from the interior of a syenitic intrusion to the andesitic host rock, each 5 m thick, it is revealed that the types of altered minerals and the content of magnetite vary greatly. The typical alteration features of the Qia'erdundasixi iron deposit are the pervasive development of diopside with minor andradite. The grain sizes of clinopyroxene and feldspar phenocrysts of syenite decrease significantly near the contact zone of the syenite pluton, indicative of quenching. Magnetite mineralization mainly develops in magnetite-quartz veins in the outer contact zone of syenite.

Alteration Stages

Based on field and microscopic observations, the magnetite mineralization can be divided into the skarn, quartz-sulfide, and supergene stages (Figure 3). The skarn stage includes the prograde and retrograde skarn stages. The minerals in the prograde skarn stage are composed of diopside + augite + andradite + magnetite + calcite + quartz. In the internal contact zone between syenite and intermediate-basic volcanic rocks, abundant fine-grained diopside and magnetite develop

around the primary salite. These clinopyroxenes are densely disseminated or are present as veinlets near the contact zone (Figure 4A), whereas magnetite is sparsely disseminated or in veinlets (Figures 4B, C). Andradite has been substituted by chlorite through pseudomorphism in the later stage.

The minerals in the retrograde skarn stage are composed of epidote + chlorite + actinolite + K-feldspar + calcite + magnetite + quartz + andradite, which are developed both in the internal and external contact zone. Clinopyroxene is commonly metasomatized by epidote + chlorite + magnetite, and epidote and chlorite alterations in the outer contact zone are well developed (Figure 4D). At this stage, abundant magnetite develops in the outer contact zone in a densely disseminated manner, becoming the main ore. Alteration of quartz + magnetite + K-feldspar + calcite + sericite + chlorite + prehnite + actinolite + chalcopyrite + pyrite is developed in the quartz-sulfide stage (Figures 4E-I). A quartz-magnetite vein with a width of about 2–10 cm is the typical feature of this stage, where magnetite accounts for as much as 40 vol% of the vein volume (Figures 4F, G). Chalcopyrite is disseminated and magnetite is metasomatized by hematite, and reflected light (Figure 4J). Minerals of the hydrothermal period are developed both in the internal and external contact zones. The grain size of K-feldspar is coarse, with inclusions of diopside formed in the early stage (Figures 4K-L). The calcite vein formed in the latest stage cuts through the early-stage magnetite (Figure 4M). Malachite is also developed in

TABLE 1 | Zircon SHRIMP dating results for the Qia'er dunbasixi syenites.

206Pb/c	U	Th	232Th/ 238U	206Pb*/ 238U		207Pb/ 206Pb		Total	Error	238U/ 206Pb	Error	207Pb/ 206Pb*		Error	206Pb*/ 238U	Error	207Pb*/ 238U	Error	206Pb*/ 238U	Error	Correlation
				Age, Ma	Ma	Age, Ma	Ma					%	%								
1.1	0	271	137	0.52	12.8	343.5	2.2	18.27	0.65	18.27	0.65	0.05654	1.7	0.4266	1.8	0.05472	0.65	0.365			
2.1	0.71	314	178	0.59	14.6	337.5	2.2	18.47	0.61	18.61	0.67	0.0529	4.3	0.392	4.3	0.05375	0.67	0.154			
3.1	0.03	668	222	0.34	180		1751.5	3.193	0.39	3.194	0.39	0.10737	0.43	4.626	0.58	0.31310	0.39	0.674			
4.1	0.32	305	243	0.82	14.6	348.5	2.2	17.94	0.63	18	0.66	0.0514	3.3	0.394	3.4	0.05556	0.66	0.194			
5.1	0.13	365	185	0.52	16.5	330.5	1.9	18.99	0.55	19.01	0.58	0.0539	3.3	0.391	3.3	0.05260	0.58	0.177			
6.1	0.31	902	226	0.26	28.5	232.0	0.97	27.2	0.41	27.29	0.42	0.0532	2.1	0.2689	2.2	0.03665	0.42	0.194			
7.1	0.24	393	232	0.61	18.5	343.2	1.9	18.242	0.54	18.29	0.58	0.0542	3.1	0.408	3.2	0.05469	0.58	0.182			
8.1	--	191	266	1.44	32.8		1.383	4.988	1.10	4.985	1.1	0.08801	0.95	2.434	1.4	0.20060	1.10	0.752			
9.1	--	296	160	0.56	14	345.9	2.3	18.14	0.69	18.14	0.69	0.05672	1.6	0.4313	1.7	0.05512	0.69	0.403			
10.1	0.98	189	99	0.54	8.82	336.9	2.9	18.46	0.79	18.64	0.89	0.0524	7.2	0.388	7.3	0.05365	0.89	0.123			

the magnetite–quartz vein (Figure 4N), showing the overprint of secondary oxidation. The wall rock of andesite is intensely mineralized with magnetite (Figure 4O).

SAMPLING AND ANALYTICAL METHODS

In this study, Sr–Nd isotopic analysis and electron microprobe analysis of the main minerals were carried out for syenite and diorite in the study area, as well as U–Pb dating of zircon in syenite. All samples numbered 07TS187, 07TS189, 07TS190, 07TS193, 07TS194, 07TS199, FH14, FH19, FH21, FH26, and ZK07–33 were collected from the drill holes shown in Figure 2, and sampling depths were between 20 and 40 m. Ten U–Pb ages of zircon from syenite in drill hole 194 were analyzed. The Sr–Nd isotopic analysis was carried out on five syenite and four diorite samples from different drill holes. Minerals such as andradite, epidote, chlorite, sericite, and prehnite were analyzed by EPMA.

Zircon was selected under a microscope and Cathodoluminescence (CL) images were taken of it using a CAMECA SX–50 microprobe. The zircon was dated using the SHRIMP II in Curtin University of Technology at the Beijing SHRIMP Center using the SHRIMP Remote Operation System, and the data correction was based on Williams (1998).

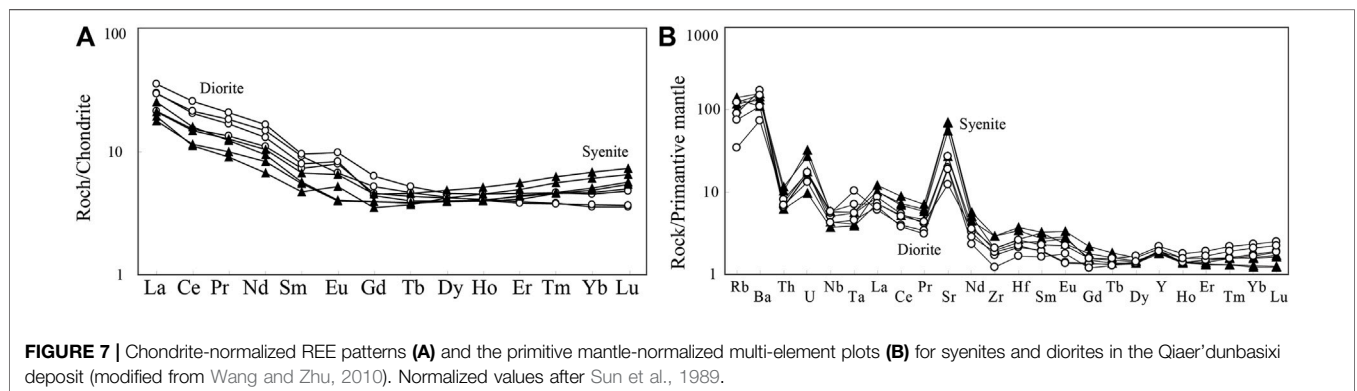
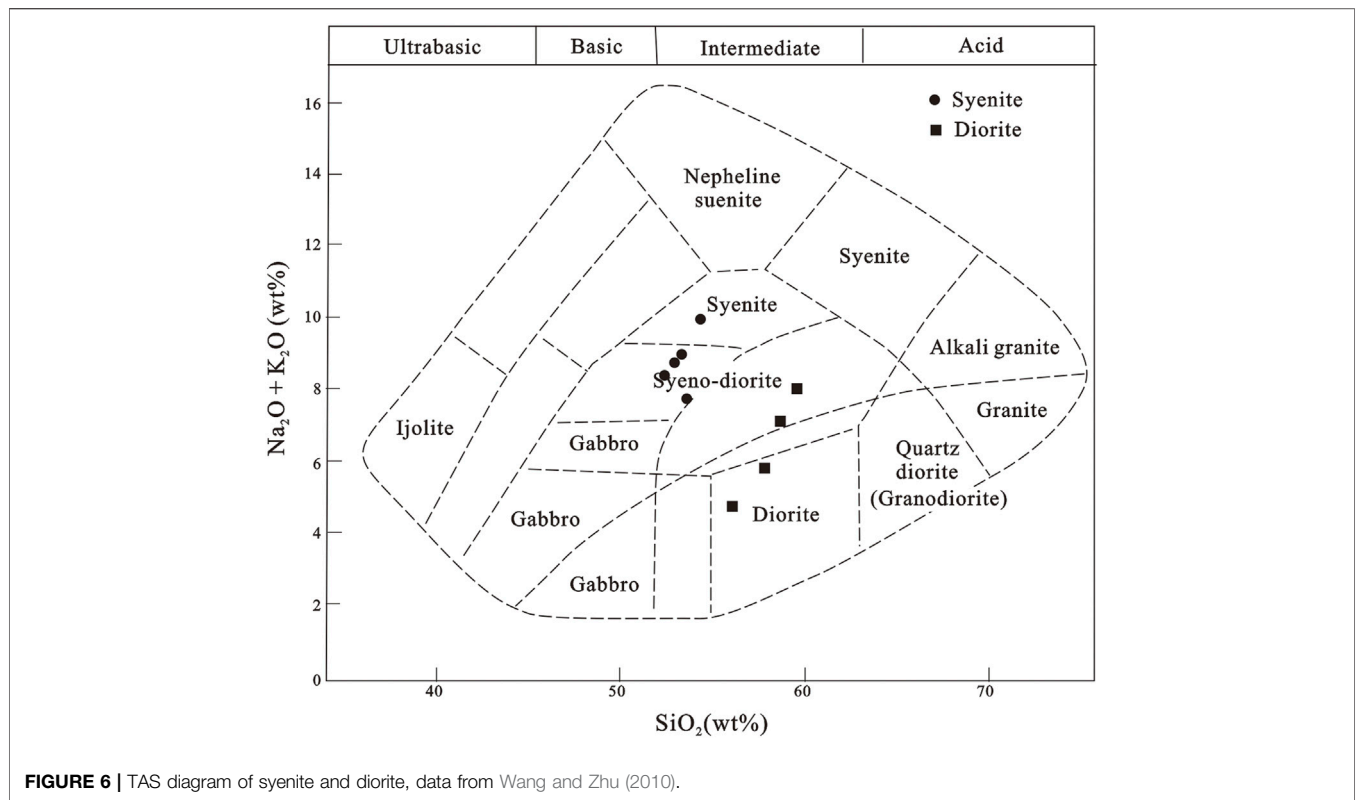
Major element compositions of minerals were measured by an electron probe microanalysis (EPMA) on a JEOL Superprobe JXA 8100 at Peking University. Operating conditions include an accelerating voltage of 15 kV, beam current 1×10^{-8} A, and spot diameter of 1 μ m. Counting times were 20s on the background position and peaked for each element. Standard specimens used natural minerals (albite for NaKa, orthoclase for KKa, wollastonite for SiKa and CaKa, hematite for FeKa, rhodonite for MnKa, and rutile for TiKa) and synthetic oxides (Al₂O₃ for AlKa, MgO for MgKa, Cr₂O₃ for CrKa, and NiO for NiKa).

An Sr–Nd isotopic analysis was conducted at the Isotope Geology Lab, Chinese Academy of Geological Science (Beijing). Sr and Nd isotopic measurements were carried out using a MC–ICP–MS (MAT-262). NBS987 ratio of ⁸⁷Sr/⁸⁶Sr = 0.71024 ± 2 (2c); the measurement accuracy of the Rb/Sr ratio was better than 0.1%, the mass fractionation of Sr isotopes was corrected using ⁸⁸Sr/⁸⁶Sr = 8.37521; Jndi-1 ratio of ¹⁴³Nd/¹⁴⁴Nd = 0.511,126 ± 6 (2c), measurement accuracy of the Sm/Nd ratio was better than 0.1%, and the mass fractionation of Nd isotopes was corrected using ¹⁴⁶Nd/¹⁴⁴Nd = 0.7219.

ANALYTICAL RESULTS

SHRIMP U–Pb Ages

The strata mainly comprised of basalt, andesite, tuff, and breccia volcanic rock outcrops in Qia'er dunbasixi belonging to Part II of the Burjin group, which were intruded by syenitic and dioritic plutons. The zircons separated from syenite show sector texture or core–mantle texture on CL images (Figure 5A). The oldest apparent age is 1751.5 Ma (spot 3.1, Th/U = 0.34, see Table 1), and one zircon sample exhibited an extremely young age (spot



6.1, 232 Ma, see **Table 1**). Most zircons constitute a concordant age and give a weighted mean age of 345 ± 2.2 Ma (MSWD = 1.3, **Figure 5C**) with Th/U ratios of 0.52–0.82 (**Table 1**).

Whole Rock Sr–Nd Isotopic Result

Whole rock major and trace element compositions of syenite and diorite have been reported in Wang and Zhu (2010). They have similar SiO₂ contents, but syenites have higher Na₂O + K₂O contents (**Figure 6**). They belong to the calc-alkaline to high-K calc-alkaline series. Syenites enrich LILE such as Rb, Ba, and Sr, and deplete HFSE such as Th, Nb, Ta, Zr, Hf, and HREE (**Figure 7**). Furthermore, a Ce-negative anomaly and Eu-positive anomaly are present. The $\epsilon_{Nd(345Ma)}$ varies from 5.5 to

6.8, with a weighted average value of 6.14 (n = 5). The ratios of (⁸⁷Sr/⁸⁶Sr)_i are between 0.704,034–0.704,197.

Diorites enrich LILE such as Rb, Ba, and Sr, and deplete HFSE such as Th, Nb, Ta, Zr, Hf, and HREE. Furthermore, a Ce-negative anomaly is present and an Eu anomaly varies (**Figure 7**). The $\epsilon_{Nd(345Ma)}$ varies from 4.6 to 5.0 with a weighted average value of 4.8 (n = 4). The ratios of (⁸⁷Sr/⁸⁶Sr)_i are between 0.704,086–0.704,114.

Skarn and Ore Mineral Chemistry

The EPMA data of main minerals during magnetite mineralization are shown in **Table 2**; **Table 3**. Minerals formed in the prograde skarn stage of the Qia'er'dunbasixi

TABLE 2 | Major element abundances (wt%) of andradite, epidote, chlorite, sericite, and prehnite.

Comment	Andradite	Epidote	Epidote	Chlorite	Chlorite	Chlorite	Sericite	Prehnite
SiO ₂	35.77	37.58	37.94	28.36	28.82	30.12	49.09	43.07
Al ₂ O ₃	0.01	25.33	26.63	14.64	15.26	17.29	30.56	23.37
FeO _t	27.15	9.68	7.36	20.34	19.70	20.05	1.85	2.11
CaO	33.17	22.97	22.55	0.09	0.07	0.37	0.05	26.77
MgO	0.05	0.01	0.05	22.67	22.10	16.67	1.59	0.36
K ₂ O	0	0.01	0	0	0	0.57	10.84	0.01
Na ₂ O	0.01	0.03	0.06	0	0.03	0.04	0.30	0
MnO	0.16	0.61	0.56	1.00	0.95	0.64	0	0.06
TiO ₂	0.02	0.04	0.04	0.25	0.20	1.21	0.03	0
Total	96.43	96.26	95.19	87.59	87.25	87.09	94.31	95.76
	O = 12	O = 12.5	O = 12.6	O = 14	O = 14	O = 14	O = 22	O = 11
Si	3.03	2.99	3.02	2.95	2.99	3.11	6.61	2.97
Al ^{IV}	0	0.01	0	1.05	1.01	0.89	1.39	0.03
Al ^{VI}	0	2.37	2.50	0.75	0.85	1.22	3.46	1.87
Ti	0	0	0	0.02	0.02	0.09	0	0
Fe ³⁺	1.93	0.64	0.49	0	0	0	0	0.12
Mg	0.01	0	0	3.52	3.41	2.57	0.32	0.04
Fe ²⁺	0	0	0.01	1.77	1.71	1.73	0.21	0
Mn	0.01	0.03	0.03	0.07	0.07	0.04	0	0
Ca	3.02	1.96	1.92	0.01	0.01	0.04	0.01	1.98
K	0	0	0	0	0	0	1.86	0
Na	0	0	0.01	0	0	0.01	0.08	0
Sum	8.00	8.00	7.98	10.13	10.07	9.71	13.93	7.02

deposit mainly include diopside + augite + andradite + magnetite + calcite + quartz. Andradite has a low SiO₂ content (35.77 wt%) and nearly no Al₂O₃ content (0.01 wt%) as well as MnO content (0.16 wt%). Epidotes formed in the retrograde skarn stage have SiO₂ contents of 37.58–37.94 wt%. The Al₂O₃ and MnO contents of the epidotes are within 25.33–26.63 wt% and 0.56–0.61 wt%, respectively. Chlorite belongs to pycnochlorite based on their Si–Fe contents (SiO₂ = 28.36–30.12 wt%, FeO_t = 19.70–20.34 wt%). Sericite has Al₂O₃ of 30.56 wt% with Si/Al^{IV} ratio of 4.76, classifying it as phengite. Prehnite with CaO of 26.77 wt% is mainly formed in the quartz–sulfide stage. Magnetite in the mining area contains certain amounts of V and Ti, and can be divided into three generations: magnetite in the clinopyroxene phenocryst (Figures 4A, B), magnetite in the syenite matrix (Figures 4C, D), and magnetite in the hydrothermal vein (Figures 4F, G). The magnetite inclusion in clinopyroxene has Fe³⁺/ΣFe of 0.53–0.65, with a little Al₂O₃ (0.07–0.31 wt%). From the core to the rim of clinopyroxene, the TiO₂ of magnetite inclusions decreases from 12.78 wt% to 0.21 wt%, and Fe³⁺/ΣFe ratios increase from 0.53 to 0.60, indicating that the oxygen fugacity gradually increases with the crystallization evolution of magma. Some magnetite inclusions in clinopyroxene contain up to 12.78 wt% TiO₂ (Table 3). The magnetite in the matrix contains low Ti, with Fe³⁺/ΣFe ratios being 0.64–0.66. Magnetite in the quartz vein contains nearly no Ti. The content of Ti is a sensitive indicator of the origin of magnetite: magnetite of magmatic origin normally has the highest content of Ti and often forms titanomagnetite, whose TiO₂ composition can be 12–16%. The content of Ti in its composition decreases significantly when contacting metasomatic or hydrothermal origin magnetite. For magnetites of the sedimentary

metamorphic origin, the content of Ti is the lowest. In this study, the magnetite in clinopyroxene contains up to 12.78 wt% TiO₂, indicating a magmatic origin. This is also evidenced in Figure 8 where they generally fall within the area of magmatic magnetite. Magnetite in the magnetite–quartz vein falls into the “skarn type” (Figure 8B) and “hydrothermal type” (Figure 8C) of the “contact metasomatic magnetite area” (Figure 8A), showing the characteristic of the skarn type. At last, magnetite in the syenite matrix is relatively complex and generally belongs to magmatic magnetite (Figure 8).

DISCUSSION

Geochronology

Magnetite mineralization occurs in both the internal and external contact zones of syenite, and therefore is closely associated with the emplacement of the syenite pluton. We suggest that the crystallization age of the syenite pluton corresponds to the metallogenic age of the Qia'er dunbasixi iron deposit. Zircons from syenite generally have typical magmatic oscillatory zoning. Some zircons show a fan-shaped structure and a few zircons have a core–mantle structure. The apparent age of the oldest zircon is 1751.5 Ma (measuring point three.1, Th/U = 0.34), and the other zircon exhibits the age of Mesoproterozoic (1,383 Ma, measuring point 8.1, Th/U = 1.44). On the contrary, point 6.1 indicates an abnormally young zircon (232 Ma, Th/U = 0.26). In addition to these three measuring points, the other seven zircons give a relatively consistent concordia age, with a weighted average of 345 ± 2.2 Ma (MSWD = 1.3, Figure 5). The variation of zircon Th/U ratios is also relatively limited (0.52–0.82). We suggest that this mean age (345 ± 2.2 Ma) represents the crystallization age of

TABLE 3 | Major element abundances (wt%) of magnetites (c: core; r: rim).

Sample	187-5	187-6	187-11	187-7	187-8	187-9	187-10	187-1	187-2	187-3	187-4	FH26-1	FH26-2	FH26-3	FH26-4
Location	Cpx	Cpx	Cpx	Cpx	Mantle	matrix	matrix	matrix	matrix	matrix	matrix	vein	vein	vein	vein
Position	r	r	c	r	-	-	-	-	-	-	-	-	-	-	-
SiO ₂	0.01	0	0.02	0.08	0.08	0.04	0.03	0.07	0.06	0.06	0.07	0.07	0.06	0.11	0.02
TiO ₂	0.39	0.21	12.78	4.28	2.15	0.10	0.09	0.08	0.07	0.11	0	0.01	0	0.01	0.02
Al ₂ O ₃	0.26	0.07	0.09	0.31	0.28	0	0	0.02	0.01	0	0	0	0	0	0
Cr ₂ O ₃	4.39	4.47	1.72	2.27	1.94	1.99	1.34	5.26	5.64	6.32	6.20	0	0.08	0.21	0.17
FeO _t	88.54	91.57	78.50	86.61	85.54	87.71	92.15	91.79	90.50	90.48	90.67	91.57	91.01	89.38	90.02
MnO	0	0.16	0.20	0	0.02	0.16	0.09	0.01	0	0	0.07	0	0.06	0	0.02
MgO	0.02	0.07	0.25	0.03	0.02	0.01	0	0.03	0.03	0.02	0.02	0	0.05	0.10	0.13
CaO	0	0	0.01	0.15	0.26	0.16	0	0.04	0.05	0.07	0.16	0	0.20	0.61	0.48
O = 32															
Si	0	0	0.01	0.02	0.03	0.01	0.01	0.02	0.02	0.02	0.02	0.02	0.02	0.03	0.01
Ti	0.09	0.05	2.98	0.99	0.51	0.02	0.02	0.02	0.02	0.02	0	0	0	0	0
Al	0.09	0.02	0.03	0.11	0.11	0	0	0.01	0	0	0	0	0	0	0
Cr	1.07	1.05	0.42	0.55	0.49	0.50	0.32	1.23	1.33	1.48	1.45	0	0.02	0.05	0.04
Fe ³⁺	14.65	14.83	9.56	13.31	14.33	15.43	15.62	14.69	14.60	14.43	14.51	15.95	15.94	15.87	15.94
Fe ²⁺	8.08	7.98	10.82	8.95	8.44	7.93	8.01	8.01	8.00	8.01	7.94	8.02	7.91	7.78	7.78
Mn	0	0.04	0.05	0	0.01	0.04	0.02	0	0	0	0.02	0	0.02	0	0.01
Mg	0.01	0.03	0.12	0.01	0.01	0	0	0.01	0.01	0.01	0.01	0	0.02	0.05	0.06
Ca	0	0	0	0.05	0.09	0.05	0	0.01	0.02	0.02	0.05	0	0.07	0.21	0.16
Fe ³⁺ /(Fe ³⁺ +Fe ²⁺)	0.64	0.65	0.53	0.60	0.63	0.66	0.66	0.65	0.65	0.64	0.65	0.67	0.67	0.67	0.67

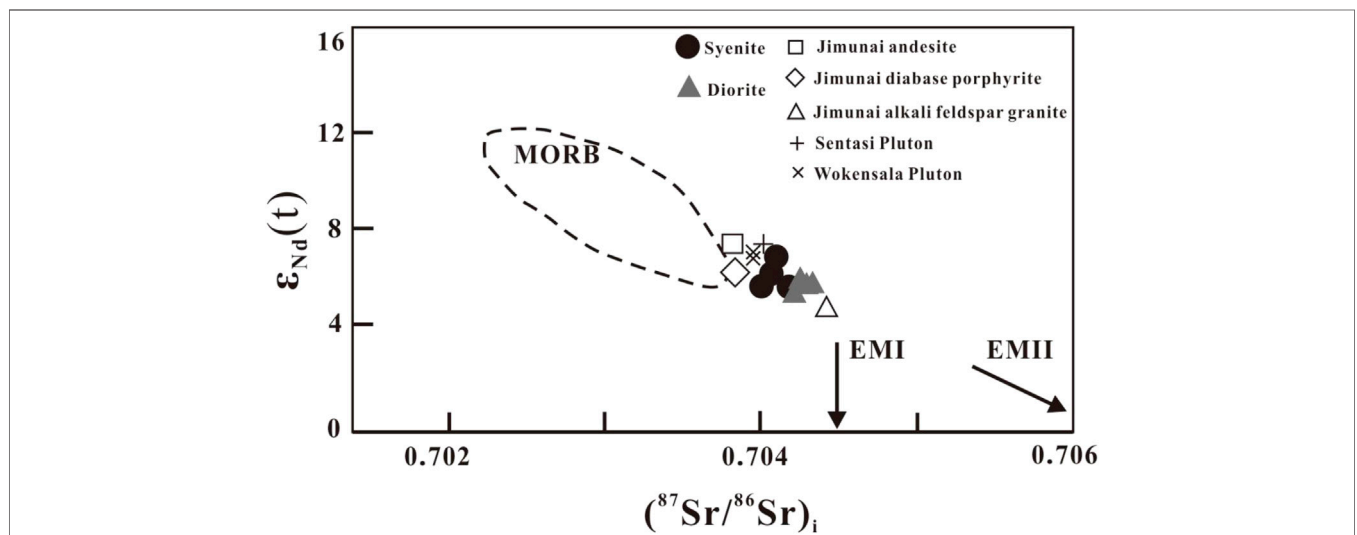


FIGURE 8 | $\epsilon_{Nd}(t)$ vs. $(^{87}Sr/^{86}Sr)_i$ plot for syenite and diorite in Qia'erdundunbasixi deposit. The field for MORB is from Zou et al. (2000) and Barry and Kent (1998), EMI and EMII are from Zindler and Hart (1986). Jimunai andesite, sillite and alkali–feldspar granite are from He et al. (1994), Sentasi and Wokensala intrusions are from Yuan et al. (2006).

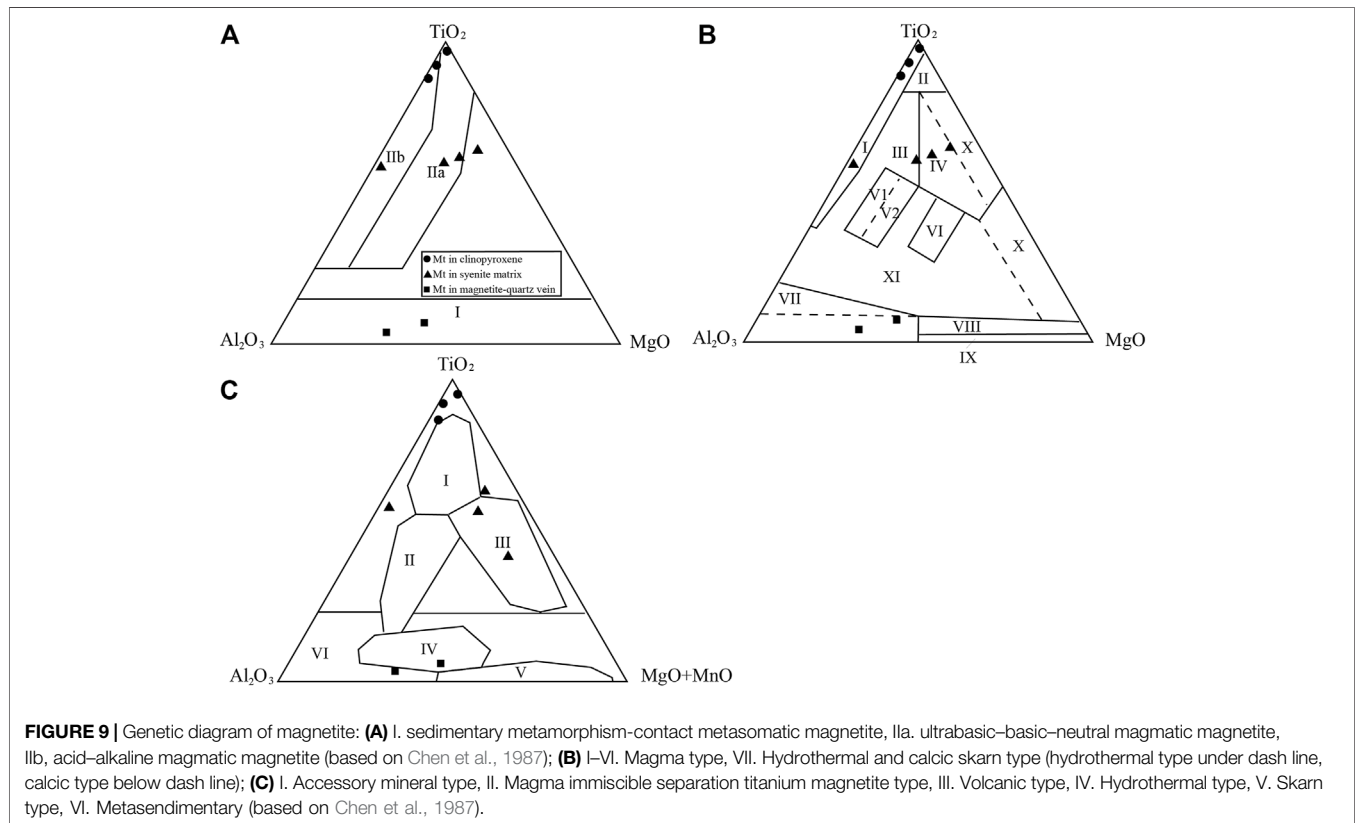
syenite, and Proterozoic zircon should be the residue of magma source material. The young age (232 Ma) obtained at point 6.1 is significantly different from other early Carboniferous zircons by its abnormally low Th/U ratio. We estimate that there is no geological significance, but it is possibly the result of the destruction of magmatic zircon by metallogenic hydrothermal fluid, which is similar to zircon in granite transformed by a ductile shear zone (Zhu and Song, 2006).

Petrogenesis and Geodynamic Setting

The intrusive rocks in the Qia'erdundunbasixi mining area are syenite, diorite, and granodiorite. They have calc–alkaline island arc–like compositions with a distinctive light and heavy rare earth differentiation, and are enriched in large ion lithophile elements and depleted in high field strength elements such as Nb, Ta, Zr, and Hf (Wang and Zhu, 2010). Syenite has high $\epsilon_{Nd}(t)$ (+5.5–+6.8) and relatively low $(^{87}Sr/^{86}Sr)_i$

TABLE 4 | Sr–Nd isotopic composition for the intrusive rocks in the Qia'erdubasixi deposit.

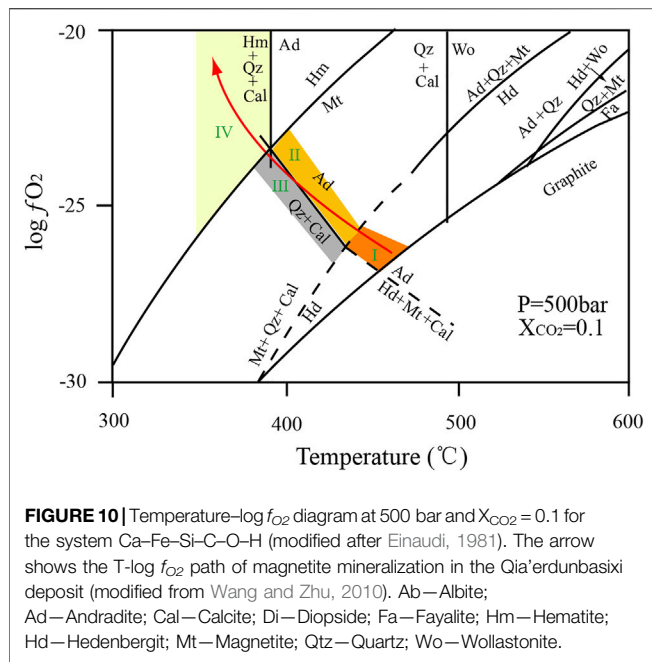
Sample	07TS187	07TS190	07TS193	FH14	07TS189	07TS199	FH21	FH19	ZK07-33
Lithology	Syenite	Syenite	Syenite	Syenite	Syenite	Diorite	Diorite	Diorite	Diorite
$^{87}\text{Rb}/^{86}\text{Sr}$	N.A	0.179695	0.161246	0.166444	N.A	0.235611	0.253706	N.A	0.315731
$^{87}\text{Sr}/^{86}\text{Sr}$	N.A	0.705,079	0.704,885	0.704,851	N.A	0.705,396	0.70589	N.A	0.705,893
(2σ)	N.A	0.000021	0.000012	0.00001	N.A	0.00001	0.000012	N.A	0.00001
$(^{87}\text{Sr}/^{86}\text{Sr})_i$		0.704197	0.704093	0.704034		0.704109	0.704086		0.704114
$^{147}\text{Sm}/^{144}\text{Nd}$	0.116,442	0.105983	0.108047	0.106275	0.115034	0.123978	0.115478	0.125954	0.126571
$^{143}\text{Nd}/^{144}\text{Nd}$	0.512,794	0.512731	0.512747	0.512717	0.5128	0.512711	0.51271	0.512715	0.512737
(2σ)	0.000010	0.000013	0.000012	0.000013	0.000013	0.000014	0.000013	0.000012	0.000012
$\epsilon_{\text{Nd}}(345\text{Ma})$	6.6	5.8	6	5.5	6.8	4.6	5	4.6	5



(0.7040–0.7042) as shown in the $(^{87}\text{Sr}/^{86}\text{Sr})_i - \epsilon_{\text{Nd}}(t)$ diagram (Table 4; Figure 9), which generally indicates a mantle source with a certain amount of assimilation of crustal materials. A previous Sr–Nd isotopic analysis of the magmatic rocks in the Sawur area shows that they all have low $(^{87}\text{Sr}/^{86}\text{Sr})_i$ and high $\epsilon_{\text{Nd}}(t)$ and are relatively uniform ($(^{87}\text{Sr}/^{86}\text{Sr})_i = 0.7035\text{--}0.7046$, $\epsilon_{\text{Nd}}(t) = +5.7\text{--}+8.0$) (He, 1994; Yuan et al., 2006; Zhou et al., 2006). Their depleted model ages are concentrated between 500 and 700 Ma with small variations, indicating a young magma source. All these lines of evidence suggest that the Sawur area was an island arc setting in at least the Early Carboniferous.

Microfossils in silicic rocks in the Char ophiolite confirm the existence of the Ertix–Zhaisang ocean between Altay and Kazakhstan from the Devonian to Early Carboniferous (Iwata

et al., 1994, 1997; Zheng et al., 2021), and therefore the Zarma–Sawur volcanic arc on the northeast edge of the Kazakhstan plate is thought to be the product of southward subduction of the Ertix–Zhaisang ocean (Demidenko & Morozov, 1999; Vladimirov et al., 2008; Chen et al., 2019; Duan et al., 2019). The intrusions near the Sawur Mountain in the Early Carboniferous may represent the island arc magmatism triggered by the southward subduction of the Ertix–Zhaisang ocean, which is a part of the Zarma–Sawur Island arc (Chen et al., 2010). Calc–alkaline andesitic lavas, andesitic breccias, pyroclastic rocks, and subvolcanic rocks are widely exposed in the Kuoerzhenkuola and Buerkesidai mining areas in the Sawur area. The age of the andesite measured by the Rb–Sr method is 347–343 Ma (Liu et al., 2003). Both gold deposits are in the same volcanic system, belonging to the Lower Carboniferous Heishantou

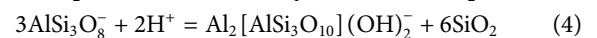
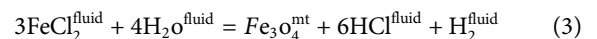
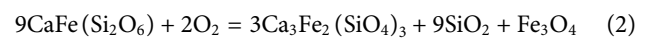
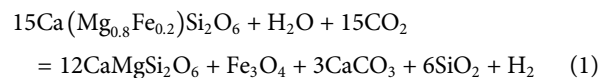


Formation. A geochemical analysis of this set of volcanic rock also corresponds with the island arc setting (Shen et al., 2005, 2007).

Skarn Evolution and Mineralization

In the prograde skarn stage, the salite in the syenite was altered into diopside and magnetite (Figure 10) (formula 1). There are two generations of andradite. The andradite in the early stage coexists with hedenbergite and calcite, with a temperature range of 450–500 °C (Figure 10). Then, the hedenbergite breaks into andradite, quartz, and magnetite, suggesting an increase in the oxygen fugacity and a decrease in temperature of the metallogenic environment (Figure 10) (formula 2). In the retrograde skarn stage, the salite was metasomatized by epidote and chlorite, and fine-grained magnetite was precipitated resulting in actinolite. Chou and Eugster (1977) suggested that iron

circulates in the form of ferrous chloride ($FeCl_2$) in supercritical fluid with an absence of S and the presence of Cl (Formula 3). The hydrochloric acid generated from the reaction dissolves the precipitated magnetite, and to drive the reaction in the direction of magnetite formation, conditions which neutralize hydrochloric acid must exist. The sericitization of feldspar in syenite is developed mostly in the early stage; sericitization of feldspar can consume H^+ and promote the formation of magnetites (formula 4). A large quantity of magnetite and quartz forms veins which constitute the main ore body. The magnetite at this stage is highly euhedral, and lath-shaped, accounting for about 50 vol% of the veins (Figures 4F, G), and the formation temperature is below 400 °C (Figure 10). This process mainly occurs in the quartz–sulfide stage, and is accompanied by a strong potassic alteration.



Comparisons With Other Skarn Deposits

A comparison between the Qia'erdundasixi Fe deposit and a typical skarn deposit is listed in Table 5. In contrast to typical skarn deposits, the Qia'erdundasixi deposit has weak skarn mineralization and small reserves. In the island arc setting, mafic magma pools and interacts with crustal rock in the MASH zone, with the generation of less dense, hybrid, andesitic–dacitic magma that associates with Cu mineralization. Consequently, the relatively mafic magmas ascend and trigger the Fe skarn mineralization in the Sawur volcanic rocks (Figure 11). Einaudi et al. (1981) proposed that skarn with volcanic rocks as the wall rocks belongs to the metasomatic skarn, which is the result of large-scale magmatic hydrothermal fluid infiltrates which react with volcanic rocks. The properties of hydrothermal fluid are the major controlling factor (Einaudi et al., 1981). Zhao et al. (1990) referred to these deposits as skarn deposits related to volcanic gas–liquid interaction,

TABLE 5 | Comparison between the Qia'erdundasixi Fe deposit and a typical skarn deposit (Meinert et al., 2005; Chang et al., 2019).

	Typical skarn Deposit	Qia'erdundasixi Fe Deposit
Country rock	Limestone, dolomitic limestone, dolomite, and other carbonate rocks	Andesite and tuff
Grade and reserves	High grade and large reserves	Rich ore and reserve unknown
Lithosome	Calcareous alkaline series: granite-granodiorite porphyry-quartz diorite-diorite; Alkaline series: alkaline syenite - granite syenite - quartz monzonite - monzonite	Syenite
Alteration	Calcium skarn: garnet, pyroxene, epidote, and actinolite; Magnesium skarn: magnesium olivine, diopside, spinel, wollastonite, serpentine, phlogopite etc.	Calcium skarn: pyroxene, garnet, epidote, chlorite etc
Mineralization	Internal and external contact zones of rock mass and bedding of country rock	Internal and external contact zone of intrusion
Orebody	Layer-like, lenticular, nest-like, columnar, vein-like, etc	Irregular veins, beaded and fine veins formed by filling and metasomatism
Ore structure	Massive, disseminated, banded, and miarolitic structure	Massive and veined, etc.
Metal	W, Cu, Fe, Mo and Zn	Fe, Cu, and Au
Tectonic environment	Oceanic island arc, continental margin, orogenic belt	Island arc
Representative deposit	Sayak, Kazakhstan, Hanxing Iron Mine, and Shouwangfen Copper Mine	Similar: Monku, Xinjiang, Merry Widow, Iron Hill, Canada

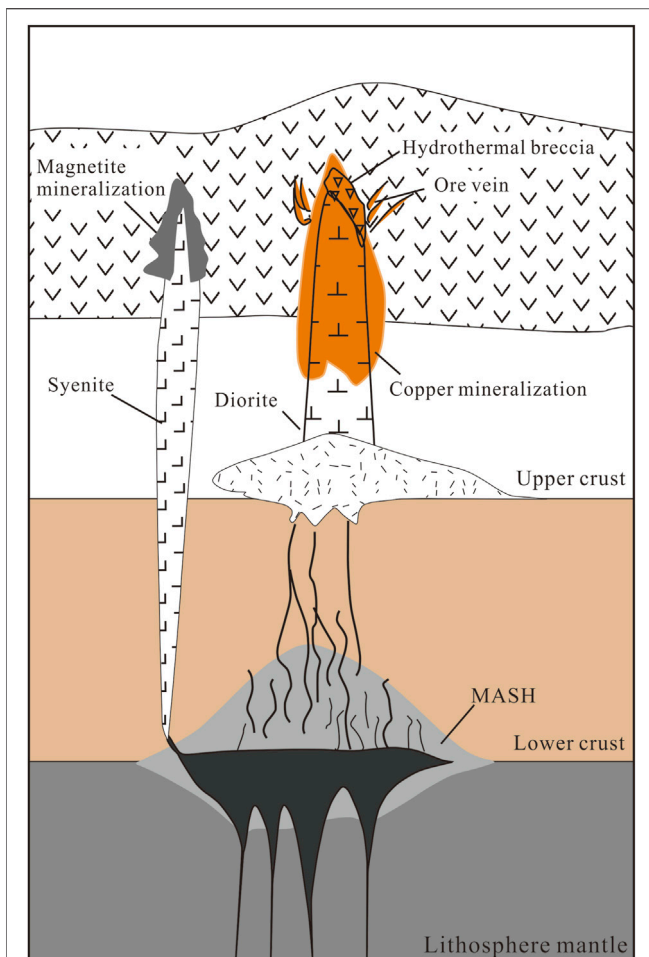


FIGURE 11 | Visualization of the MASH zone at the base of the crust, where hot, dense, mafic magmas pool and interact with crustal rocks to generate less dense, hybrid, andesitic–dacitic magmas, minor mafic magma will ascend, then exist in the form of syenites with an intense skarn alteration and magnetite mineralization. Andesitic–dacitic magma after MASH will enhance copper mineralization.

which were formed mostly by contact metasomatism by an ore-bearing volcanic gas–liquid. Skarn deposits related to volcanic wall rock are mainly calcic iron skarn deposits, which normally develop in an island arc or post-collisional environment, such as seen in Canada, China, the United States, Cuba, and Japan (Einaudi et al., 1981; Wang et al., 2020; Sun et al., 2022). The intrusions are typically diorite or syenite, both rich in iron (Ray et al., 1995), and the wall rock includes limestone and intermediate–basic volcanic rocks (Einaudi et al., 1981).

The main minerals of calcic iron skarn deposits are garnet and pyroxene, as well as minor epidote, ilvaite, and actinolite, all of which are iron-rich (Prutov et al., 1989). In addition to endoskarn alteration, intrusive rocks also extensively develop albite, K-feldspar, and scapolite (Meinert et al., 2005). There are many iron skarn deposits occurring in Triassic limestone and volcanic wall rocks reported in western Canada (Ray et al., 1995). For example, the wall rocks of Iron Hill, Iron Crown, and Merry

Widow iron deposits are limestone and volcanic rock, causing different types of skarn alterations. Generally, the skarn in limestone is more iron-rich, and the representative skarn minerals such as garnet and monoclinic pyroxene are very different. Garnet in volcanic rocks contains more Al, Mn, Mg, Ti, and V, and pyroxene also contains more Al and V, implicating significant interaction with volcanic rocks (Meinert et al., 1981). To make a comparison, further studies on the mineral chemistry of the Qia'erdundasixi deposit are required in the future.

CONCLUSION

The Qia'erdundasixi Fe–Cu deposit in Sawur is hosted by Devonian and Carboniferous volcanic rocks in an island arc setting. The ore-causative intrusions are syenite and diorite, and the SHRIMP U–Pb age of syenite is 345 ± 2.2 Ma (MSWD = 1.3). Their Sr–Nd isotopic compositions ($(^{87}\text{Sr}/^{86}\text{Sr})_i = 0.70403$ to 0.70420 and $\varepsilon_{\text{Nd}(t)} = +5.5$ to $+6.8$) as well as their REE and PM patterns all exhibit arc magma characteristics with a certain amount of crustal contamination. Magnetite and copper mineralization developed mostly along the contact zones of syenite and diorite, respectively. Magnetite mineralization shows the typical characteristics of skarn alteration, which can be divided into prograde skarn, retrograde skarn, and Quartz–sulfide stages. In contrast to the typical skarn deposits, the Qia'erdundasixi deposit has weak skarn mineralization and small reserves. Copper mineralization is concentrated along the outer contact zone of diorite, and has four stages of albite–quartz (1), chalcopyrite–pyrite–gold–seriate–quartz (2), chalcopyrite–pyrite–epidote–prehnite (3), and sphalerite–galena–quartz–calcite (4). Many magnetite, gold, and copper deposits and other mineral occurrences have been discovered in the volcanic rocks of the Sawur area, suggesting that the Devonian and Carboniferous volcanic rocks are highly susceptible to Fe, Cu, and Au mineralization.

DATA AVAILABILITY STATEMENT

The original contributions presented in the study are included in the article/Supplementary Material; further inquiries can be directed to the corresponding authors.

AUTHOR CONTRIBUTIONS

SY and RW interpreted the data and wrote the manuscript, and YZ designed the experiment and participated in the writing. Q–SZ processed the data and participated the writing.

FUNDING

Financial support was provided by the Chinese National Natural Science Foundation (Grant Nos. 92162104, 41973037, 40821002, 40572033, and 42072077).

REFERENCES

- Barry, T. L., and Kent, R. W. (1998). “Cenozoic Magmatism in Mongolia and the Origin of Central and East Asian Basalts,” in *Mantle Dynamics and Plate Interactions in East Asia, American Geophysical Union*. Editor M. F. J. Flower, S. L. Chung, C. H. Lo, and T. Y. Lee *Geodynamics* 27, 347–364.
- Bureau of Geology and Mineral Resources of Xinjiang Uygur Autonomous Region (1993). *Regional Geology of Xinjiang Uygur Autonomous Region*. Beijing: Geological Publishing House. in Chinese.
- Chen, G. Y. (1987). *Genetic and Prospecting Mineralogy* Chongqing: Chongqing Publishing House. In Chinese.
- Chen, J.-F., Han, B.-F., Ji, J.-Q., Zhang, L., Xu, Z., He, G.-Q., et al. (2010). Zircon U–Pb Ages and Tectonic Implications of Paleozoic Plutons in Northern West Junggar, North Xinjiang, China. *Lithos* 115, 137–152. doi:10.1016/j.lithos.2009.11.014
- Chen, J. F., Ma, X., Simon, A., Du, H. Y., and Liu, B. (2019). Late Ordovician to Early Silurian Calc–Alkaline Magmatism in the Xiemisitai Mountains, Northern West Junggar: a Response to the Subduction of the Junggar–Balkhash Ocean. *Int. Geol. Rev.* 61, 2000–2020. doi:10.1080/00206814.2019.1576148
- Chen, S. S., Li, P., Guo, X. J., Liu, X. F., Zhang, B., and Du, X. W. (2017). Zircon U–Pb Geochronology and Geochemistry of Monzonite in the Heishantou Gold Deposit in Sawuer Region, West Junggar and Prospecting Potential. *Geotect. Metallogenia* 41, 865–878. in Chinese.
- Chou, I.-M., and Eugster, H. P. (1977). Solubility of Magnetite in Supercritical Chloride Solutions. *Am. J. Sci.* 277, 1296–1314. doi:10.2475/ajs.277.10.1296
- Demidenko, A. N., and Morozov, O. L. (1999). Geology and Paleomagnetism of Middle–Upper Paleozoic Rocks of the Saur Ridge. *Geotectonics* 4 (4), 64–80. in Russian with English abstract.
- Duan, F., Li, Y., Zhi, Q., Yang, G., and Gao, J. (2019). Petrogenesis and Geodynamic Implications of Late Carboniferous Sanukitic Dikes from the Bieluagaxi Area of West Junggar, NW China. *J. Asian Earth Sci.* 175, 158–177. doi:10.1016/j.jseas.2019.01.013
- Einaudi, M. T., Meinert, L. D., and Newberry, R. J. (1981). Skarn Deposits. *Econ. Geol.* 75, 317–391. doi:10.5382/av75.11
- He, G. Q., Cheng, S. D., Xu, X., Li, J. Y., and Hao, J. (2005). *Geotectonic Map of Xinjiang and its Neighboring Areas, China 1:1500000*. Beijing: Geological Publishing House.
- He, B. C., Tan, K. R., and Wu, Q. H. (1994). Ages and Sr, Nd Isotopic Evidences of Mantle Source Magmatite in the Bu’s Gold Deposit, Jimunai County, Northern Xinjiang. *Geotect. Metallogenia* 18, 219–228.
- He, G. Q., Liu, D. Q., Li, M. S., Tang, Y. L., and Zhou, R. H. (1995). The Five-Stage Model of Crustal Evolution and Metallogenic Series of Chief Orogenic Belts in Xinjiang. *Xinjiang Geol.* 13, 99–180.
- Iwata, K., Obut, O. T., and Buslov, M. M. (1997). Devonian and Lower Carboniferous Radiolarian from the Chara Ophiolite Belt, East Kazakhstan. *News Osaka Micropaleontol.* 10, 27–32.
- Iwata, K., Watanabe, T., Akiyama, M., Dobretsov, N. L., and Belyaev, S. Y. (1994). Paleozoic Microfossils from the Chara Belt (Eastern Kazakhstan). *Russ. Geol. Geophys.* 35, 145–151.
- Liu, G. R., Long, Z. N., Chen, Q. Z., and Zhou, C. (2003). The Formation Age and Geochemical Characteristics of the Volcanic Rock of Kuo’erzhenkuola’s Gold Mine in Xinjiang. *Xinjiang Geol.* 21, 177–180.
- Meinert, L. D., Dipple, G. M., and Nicolescu, S. (2005). World Skarn Deposits. *Econ. Geol.* 100, 299–336. doi:10.5382/av100.11
- Meinert, L. D. (1984). Mineralogy and Petrology of Iron Skarns in Western British Columbia, Canada. *Econ. Geol.* 79, 869–882. doi:10.2113/gsecongeo.79.5.869
- Meinert, L. D. (1981). Skarns and Skarn Deposits. *Geosci. Can.* 19, 145–162.
- Purtov, V. K., Kholodnov, V. V., Anfilogov, V. N., and Nechkin, G. S. (1989). The Role of Chlorine in the Formation of Magnetite Skarns. *Int. Geol. Rev.* 31, 63–71. doi:10.1080/00206818909465861
- Ray, G. E., Webster, I. C. L., and Ettlinger, A. D. (1995). The Distribution of Skarns in British Columbia and the Chemistry and Ages of Their Related Plutonic Rocks. *Econ. Geol.* 90, 920–937. doi:10.2113/gsecongeo.90.4.920
- Shen, P., Shen, Y. C., Liu, T. B., Li, G. M., and Zeng, Q. D. (2005). Geochemistry of Ore-Forming Fluid and its Significance in Kuo’erzhenkuola Gold Field, Xinjiang. *Sci. China (Series D)*. 35, 862–869.
- Shen, P., Shen, Y., Liu, T., Li, G., and Zeng, Q. (2007). Genesis of Volcanic-Hosted Gold Deposits in the Sawur Gold Belt, Northern Xinjiang, China: Evidence from REE, Stable Isotopes, and Noble Gas Isotopes. *Ore Geol. Rev.* 32, 207–226. doi:10.1016/j.oregeorev.2006.10.005
- Shen, P., Shen, Y., Liu, T., Li, G., and Zeng, Q. (2008). Geology and Geochemistry of the Early Carboniferous Eastern Sawur Caldera Complex and Associated Gold Epithermal Mineralization, Sawur Mountains, Xinjiang, China. *J. Asian Earth Sci.* 32, 259–279. doi:10.1016/j.jseas.2007.10.004
- Sun, F., Zhang, J. B., Wang, R., Zhou, L. M., Jeon, H., Li, Y. Y., et al. (2022). Magmatic Evolution and Formation of the Giant Jiama Porphyry-Skarn Deposit in Southern Tibet. *Ore Geol. Rev.* 145. doi:10.1016/j.oregeorev.2022.104889
- Sun, S. S., and McDonough, W. F. (1989). *Chemical and Isotopic Study of Oceanic Basalts: Implications For Mantle Composition and Processes*. Geological Society of London, Special Publication 42, 313–345.
- Tan, L. G., Zhou, T. F., Yuan, F., Fan, Y., and Yue, S. C. (2007). ⁴⁰Ar–³⁹Ar Age of the Kalagang Formation Volcanic Rocks in Western Junggar. *Xinjiang* 42, 579–586. in Chinese.
- Vladimirov, A. G., Kruk, N. N., Khromykh, S. V., Polyansky, O. P., Chervov, V. V., Vladimirov, V. G., et al. (2008). Permian Magmatism and Lithospheric Deformation in the Altai Caused by Crustal and Mantle Thermal Processes. *Russ. Geol. Geophys.* 49, 468–479. doi:10.1016/j.rgg.2008.06.006
- Wang, R., Zhu, D., Wang, Q., Hou, Z., Yang, Z., Zhao, Z., et al. (2020). Porphyry Mineralization in the Tethyan Orogen. *Sci. China Earth Sci.* 63, 2042–2067. doi:10.1007/s11430-019-9609-0
- Wang, R., and Zhu, Y. F. (2010). Geology and Geochemistry of Qia’erdundasixi Fe–Cu–Au Deposit in Sawur, Northern Xinjiang. *Mineral. Deposits* 29, 229–242.
- Wang, R., and Zhu, Y. F. (2007). Geology of the Baobei Gold Deposit in Western Junggar and Zircon SHRIMP Age of its Wall-Rocks, Western Junggar (Xinjiang, NW China). *Geol. J. China Univ.* 13, 590–602.
- Williams, J. S. (1998). “U–Th–Pb Geochronology by ion Microprobe,” in *Application of Microanalytical Techniques to Understanding Mineralizing Processes* 7. doi:10.5382/Rev.07.01
- Windley, B. F., Alexeiev, D., Xiao, W., Kröner, A., and Badarch, G. (2007). Tectonic Models for Accretion of the Central Asian Orogenic Belt. *J. Geol. Soc.* 164, 31–47. doi:10.1144/0016-76492006-022
- Windley, B. F., Kröner, A., Guo, J., Qu, G., Li, Y., and Zhang, C. (2002). Neoproterozoic to Paleozoic Geology of the Altai Orogen, NW China: New Zircon Age Data and Tectonic Evolution. *J. Geol.* 110, 719–737. doi:10.1086/342866
- Xia, W. J., Wang, R., and Zhu, Y. F. (2022). Petrogenesis of Lamprophyre in Sawur, Northern Xinjiang, China: Implication for Volcanic Hosted Gold Deposits. *Ore Geol. Rev.* 144. doi:10.1016/j.oregeorev.2022.104856
- Yuan, F., Zhou, T. F., Deng, Y. F., Guo, X. J., Zhang, D. Y., Xu, C., et al. (2015). Ore-forming Type and Regional Metallogenic Regularity in the Sawuer region, West Junggar, Xinjiang. *Acta Petrol. Sin.* 31, 388–400. in Chinese.
- Yuan, F., Zhou, T. F., Tan, L. G., Fan, Y., Yang, W. P., He, L. X., et al. (2006). Isotopic Ages of the I Type Granites in West Junggar Sawuer Region. *Acta Petrol.* 22, 1238–1248.
- Zhang, R. (2016). *Geological and Genesis of Volcanic Hydrothermal Type Copper (Gold) Deposits (Points) in Taerbahatai–Sawuer Area*. West Junggar: Hefei: Hefei University of Technology. Dissertation/Master’s thesis.
- Zhao, Y. M., and Shen, W. B. (1990). *Skarn Deposits in China*. Beijing: Geological Publishing House. in Chinese.
- Zheng, Q., Xu, X., Zhang, W., Zheng, Y., Liu, Y., Kuang, X., et al. (2021). A Fossil Paleozoic Subduction-Dominated Trench–Arc–Basin System Revealed by Airborne Magnetic-Gravity Imaging in the Western Junggar, NW China. *Front. Earth Sci.* 9, 1076. doi:10.3389/feart.2021.760305
- Zhou, T., Yuan, F., Fan, Y., Zhang, D., Cooke, D., and Zhao, G. (2008). Granites in the Sawuer Region of the West Junggar, Xinjiang Province, China: Geochronological and Geochemical Characteristics and Their Geodynamic Significance. *Lithos* 106, 191–206. doi:10.1016/j.lithos.2008.06.014

- Zhou, T., Yuan, F., Tan, L., Fan, Y., and Yue, S. (2006). Geodynamic Significance of the A-type Granites in the Sawuer Region in West Junggar, Xinjiang: Rock Geochemistry and SHRIMP Zircon Age Evidence. *Sci. China Ser. D*. 49, 113–123. doi:10.1007/s11430-005-0121-7
- Zhu, Y., An, F., Feng, W., and Zhang, H. (2016). Geological Evolution and Huge Ore-Forming Belts in the Core Part of the Central Asian Metallogenic Region. *J. Earth Sci.* 27, 491–506. doi:10.1007/s12583-016-0673-7
- Zhu, Y., Chen, B., and Qiu, T. (2015). Geology and Geochemistry of the Baijiantan-Baikouquan Ophiolitic Mélanges: Implications for Geological Evolution of West Junggar, Xinjiang, NW China. *Geol. Mag.* 152, 41–69. doi:10.1017/s0016756814000168
- Zhu, Y., Chen, B., Xu, X., Qiu, T., and An, F. (2013). A New Geological Map of the Western Junggar, North Xinjiang (NW China): Implications for Paleoenvironmental Reconstruction. *Episodes* 36, 205–220. doi:10.18814/epiugs/2013/v36i3/003
- Zhu, Y. F., and Song, B. (2006). Petrology and SHRIMP Chronology of Mylonitized Tianger Granite, Xinjiang: Also about the Dating on Hydrothermal Zircon Rim in Granite. *Acta Petrol. Sin.* 22, 135–144.
- Zhu, Y. F., Xu, X., Luo, Z. H., Shen, P., Ma, H. D., Chen, X. H., et al. (2014). *Geological Evolution and Ore-Formation in the Core Part of Central Asian Metallogenic Region*. Beijing: Geological Publishing House, 1–202. in Chinese.
- Zindler, A., and Hart, S. R. (1986). Chemical geodynamics. *Ann. Rev. Earth Planet.* 14, 493–571.
- Zou, H. B., Zindler, A., Xu, X. S., and Qi, Q. (2000). Mg, Trace Element, and Nd, Sr and Pb Isotope Studies of Cenozoic Basalts in SE China: Mantle Sources, Regional Variations and Tectonic Significance. *Chem. Geol.* 171, 33–47.

Conflict of Interest: The authors declare that the research was conducted in the absence of any commercial or financial relationships that could be construed as a potential conflict of interest.

Publisher's Note: All claims expressed in this article are solely those of the authors and do not necessarily represent those of their affiliated organizations, or those of the publisher, the editors, and the reviewers. Any product that may be evaluated in this article, or claim that may be made by its manufacturer, is not guaranteed or endorsed by the publisher.

Copyright © 2022 Yang, Zhou, Wang and Zhu. This is an open-access article distributed under the terms of the Creative Commons Attribution License (CC BY). The use, distribution or reproduction in other forums is permitted, provided the original author(s) and the copyright owner(s) are credited and that the original publication in this journal is cited, in accordance with accepted academic practice. No use, distribution or reproduction is permitted which does not comply with these terms.